ARTICLE NO. 79-7034R

Transonic Axial Compressor Using Laser Anemometry and Unsteady Pressure Measurements

R. J. Dunker* and H. G. Hungenberg*
Propulsion Institute, DFVLR, Cologne, Federal Republic of Germany

A laser anemometer and high-response pressure probes were used to study in detail the complex flow in a transonic axial compressor rotor at 20,000 rpm. The investigation was aimed at providing complete data on the internal flowfield at the design speed for peak efficiency, near compressor surge, and choke. Useful information is presented on flow vectors, three-dimensional shock waves, oscillating total pressures, blade wakes, and losses downstream of the rotor.

Nomenclature

c = absolute velocity
c_u = tangential component of absolute velocity
$\dot{m}$ = reduced mass flow
Ma_c = absolute Mach number
Ma_w = relative Mach number
p_0 = total pressure
p = static pressure
PS = pressure side
r = radius
SS = suction side
T_0 = total temperature
u = tangential velocity
w = relative velocity
z = coordinate in axial direction
φ = coordinate in tangential direction
ω = total pressure loss coefficient

Subscripts

1 = inlet condition
2 = relative station
( )′ = with respect to relative system

Introduction

FLOW through a highly loaded transonic compressor is extremely complicated. It is three-dimensional and involves complex shock patterns, shock/boundary-layer interactions, flow separations, and secondary flows. The improvement of existing compressor flow models requires detailed experimental investigation of these phenomena.

High-response pressure testing techniques are now available to measure the oscillating static pressure along the compressor casing as well as the fluctuating total pressure downstream of rotating blade rows.[1-5] In addition, the nonintrusive optical velocimeters allow investigation of the compressor's internal flow by measuring the velocity vectors at any point inside of turbomachines accessible by laser light from outside. This is possible even within rotating blade rows.[6-11] These advanced techniques were used to investigate the internal flow of a single-stage transonic compressor. Some results of this detailed study are discussed in this paper.

Presented as Paper 79-7034 at the 4th International Symposium on Air Breathing Engines, Walt Disney World, Fla., April 1-6, 1979; submitted June 13, 1979; revision received Dec. 27, 1979.

Index categories: Airbreathing Propulsion; Transonic Flow.

*Research Engineer.

Test Compressor

The test compressor is a single-stage transonic axial compressor without inlet guide vanes, designed for a total pressure ratio of 1.51 and a mass flow of 17.3 kg/s at 20,260 rpm. Figure 1 shows the flow path of this stage. For the rotor with 28 blades MCA profiles were selected from hub to tip, whereas the 60 stator blades are composed of NACA-65 profiles; further details are documented in Refs. 12, 13, and 15. This transonic stage was investigated using conventional as well as advanced testing techniques. Figure 2 shows the overall performance map of this compressor with speed lines quite typical for a transonic stage.

Testing Technique

For the measurement of oscillating pressures, transducers based on quartz and semiconducter components are available with natural frequencies that are sufficiently large compared to the basic frequencies normally produced in turbomachines. Detailed information on these measurements is reported in Refs. 1-3 and 10. The fluctuating total pressure at the rotor outlet was measured using pitot probes with built-in semiconducter pickups. It is necessary that the transducer be directly built into the head of the probe with the diaphragm recessed 1-2 mm from the probe's entrance in order for the probe to be sufficiently insensitive to the variations in flow direction normally occurring at the outlet of turbomachine rotors. With the help of the synchronized sampling technique, the transducer signals were cleared of noise and reproduced as mean periodic distributions of total pressure.

The analysis of the velocity vectors within and downstream of the fast-moving rotor blade channels was performed using the L2F velocimeter. The anemometer operates stroboscopically and is controlled by a trigger and time delay unit which also allows shifting of the measurement point in the circumferential direction with reference to the rotating blades. The axial and radial position of the measurement volume can be changed easily by moving the velocimeter. The determination of the absolute velocity vector is quite accurate; the error of the velocity magnitude does not exceed ±1% and the flow direction can be determined to within ±1 deg. This is true nearly everywhere except within regions of highly fluctuating flow and in direct vicinity of the walls. Further details and the fundamentals of the L2F velocimeter are described in Refs. 10 and 11. The various positions of the measurement volume in the meridianal plane of the stage are indicated in Fig. 1 by circular symbols. Each symbol represents up to 15 measurement points over the circumferential direction from blade to blade. This is necessary to localize the shock position accurately and to analyze the rotor blade wakes in plane 16, downstream of the rotor, where the measurements of the periodic fluctuating total pressure were performed.

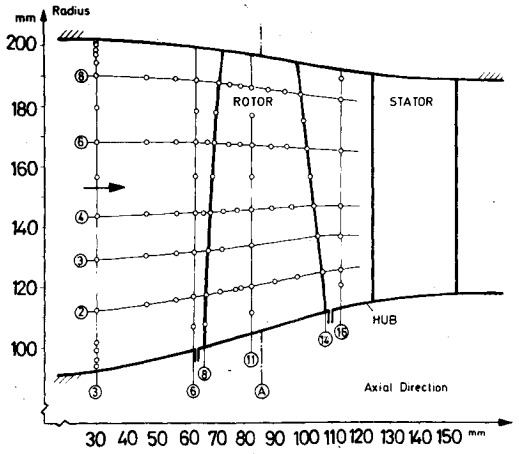

Fig. 1 Compressor flow path with measuring stations.

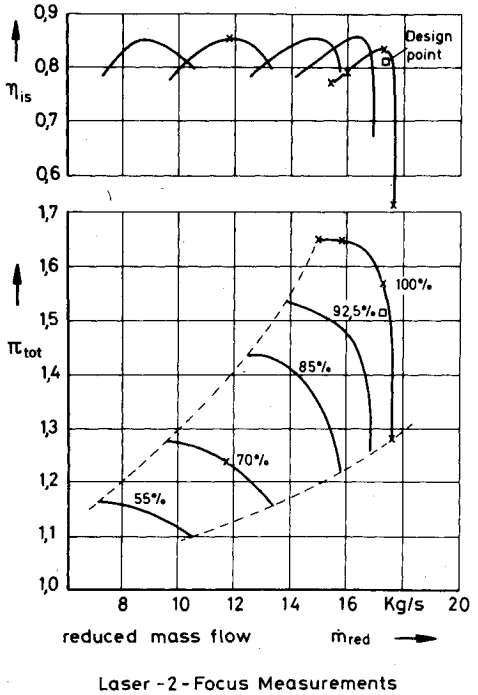

Laser-2-Focus Measurements

Fig. 2 Compressor overall performance map.

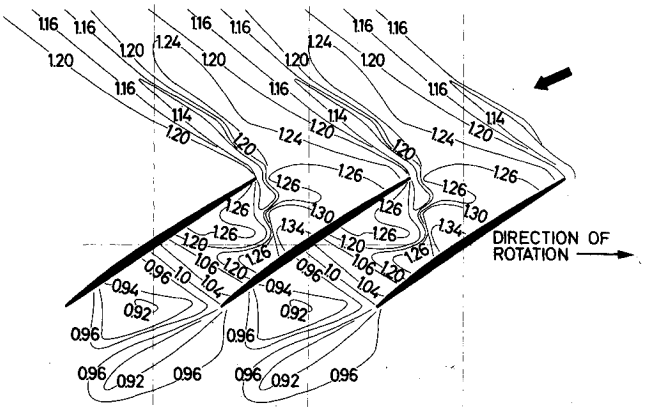

Fig. 3 Lines of constant relative Mach number on rotor blade section at 68% blade height, 100% speed, choke margin, $\dot{m} = 17.6$ kg/s.

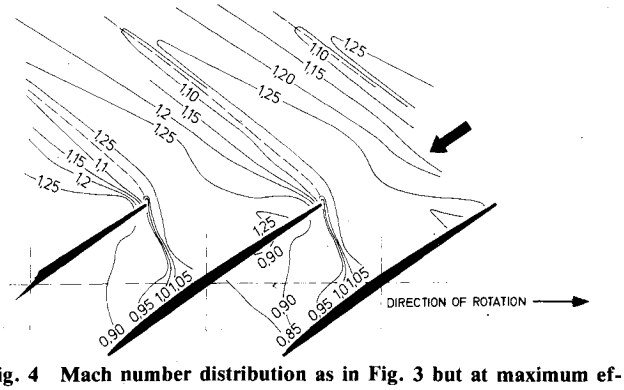

Fig. 4 Mach number distribution as in Fig. 3 but at maximum efficiency, $\dot{m} = 17.15$ kg/s.

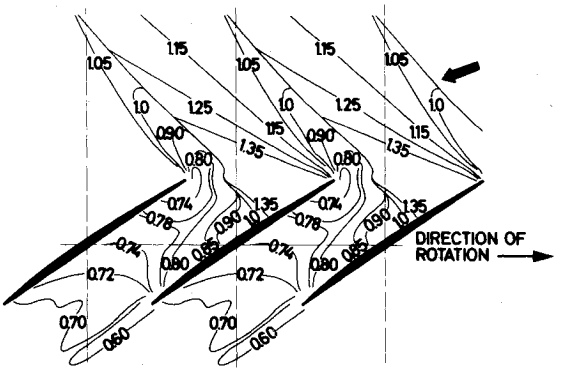

Fig. 5 Mach number distribution as in Fig. 3 but at 1.5% off compressor surge, $\dot{m} = 15.35$ kg/s.

Experimental Results and Discussion

The internal flowfield of the transonic compressor described above has already been studied using the L2F technique at the peak efficiency point at 70 and 100% of design speed. These results are documented in detail in Refs. 14-17. In this presentation, corresponding experimental results at off-design conditions along the design speed line are documented. Loss evaluation by combined analysis of velocity and unsteady total pressure measurements is emphasized.

The cross symbols on the design speed line in Fig. 2 indicate the operating points where the detailed flow studies have been performed. The symbols represent compressor operations at the choke margin (i.e., open throttle), at the compressor's best point, and at 7 and 1.5% off the surge line, respectively, with corresponding reduced mass flows of 17.6, 17.15, 15.93, and 15.35 kg/s.

The internal rotor flowfield at 68% blade height is illustrated in Figs. 3-5 as an example of flow development with throttling. Lines of constant relative Mach number are plotted over two rotor blade channels. The arrows indicate the mean inflow direction far upstream.

Figure 3 represents the flowfield at open throttle. The relative inlet Mach number is 1.184 and the meridional flow angle with respect to the axial direction is 64.5 deg. An attached shock wave appears at the blade leading edge and travels upstream interfering with the expansion waves which originate from the blade leading edge and the convex suction surface. As is typical for this low-back-pressure situation, an oblique shock exists within the blade passage impinging on the suction surface of the adjacent blade at nearly 70% chord and initiating a separation bubble (which is also confirmed in Fig. 13). The expansion waves mentioned above interact with the oblique shock and, together with the increase in flow area, cause a flow acceleration along the pressure side. Due to the back pressure, a final normal shock starts from the pressure surface and impinges on the suction surface trailing edge, causing the outlet flow to be completely subsonic. Slightly increased back pressure, produced by throttling the com-

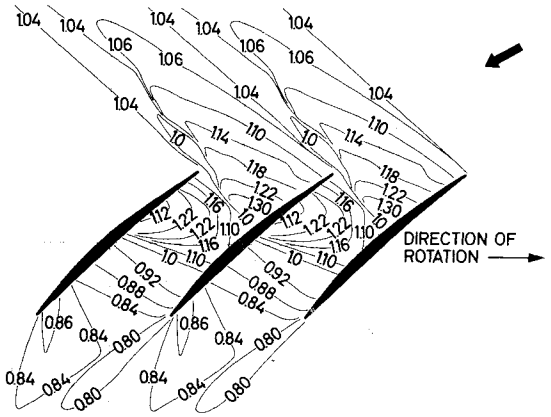

Fig. 6 Mach number distribution as in Fig. 3, however, on rotor blade section at 45% blade height, choke margin, $\dot{m} = 17.6$ kg/s.

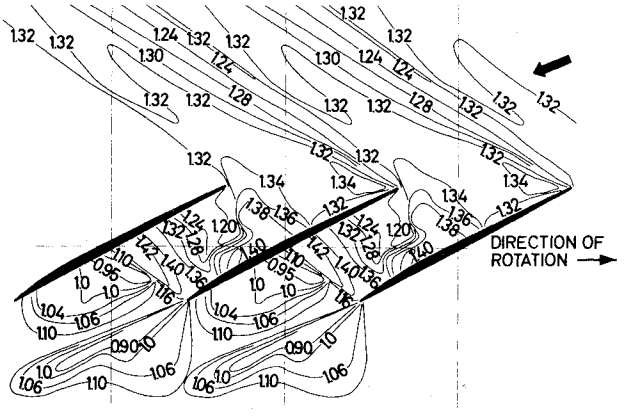

Fig. 9 Mach number distribution as in Fig. 3, but on rotor blade section at 89% blade height, choke margin, $\dot{m} = 17.6$ kg/s.

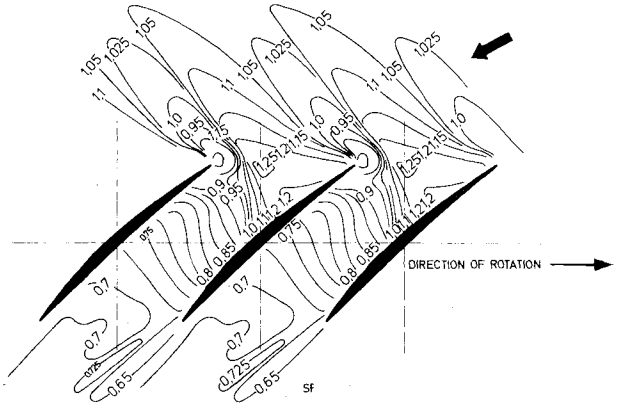

Fig. 7 Mach number distribution as in Fig. 6, but at maximum efficiency, $\dot{m} = 17.15$ kg/s.

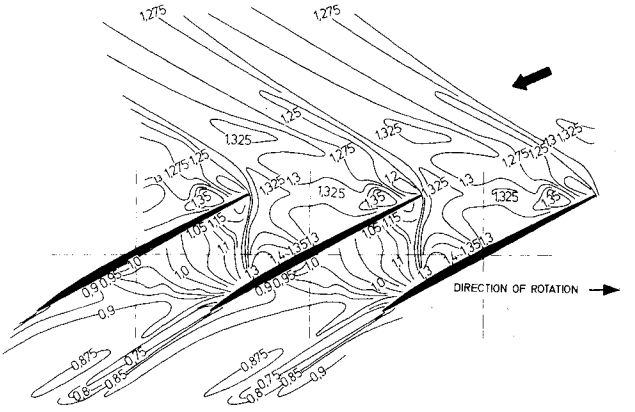

Fig. 10 Mach number distribution as in Fig. 9, but at maximum efficiency, $\dot{m} = 17.15$ kg/s.

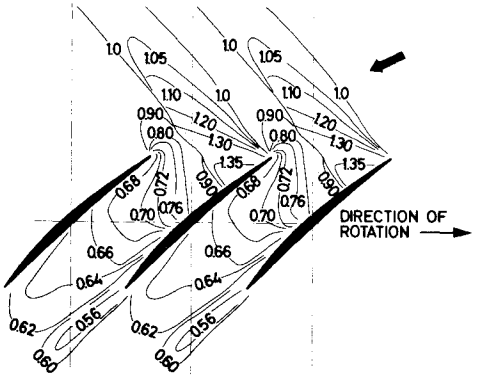

Fig. 8 Mach number distribution as in Fig. 6, but at 1.5% off compressor surge, $\dot{m} = 15.35$ kg/s.

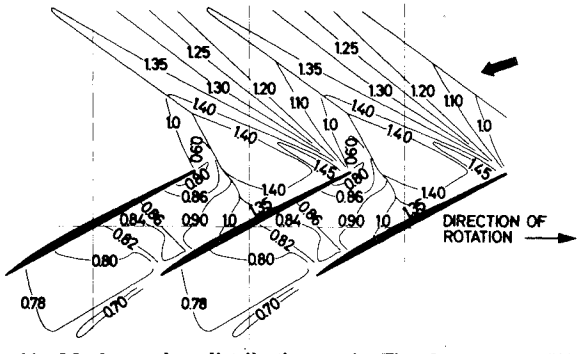

Fig. 11 Mach number distribution as in Fig. 9, but at 1.5% of compressor surge, $\dot{m} = 15.35$ kg/s.

pressor, leads to the best point flow condition as shown in Fig. 4. A typical bow shock is located ahead of each blade; its oblique branch (dashed line) travels upstream, interfering with the expansion waves emanating from leading edge and suction surface. Within the blade channel a λ shock is formed—as indicated by Mach line spreading—around 50% chord of the adjacent blade, caused by the shock/boundary-layer interaction. The subsequent flow is further decelerated by flow turning in the rear part of the blade channel. Figure 5 presents the flowfield near the surge point at design speed. The compressor is throttled to a mass flow of 15.35 kg/s, i.e., 1.5% in mass flow off surge. Due to the high positive incidence angle, a detached normal shock appears at the channel entrance with a subsonic bubble around the blade leading edge. The upstream traveling shock wave is now affected by stream-tube convergence, i.e., increasing axial velocity with axial coordinate; therefore, it bends slightly toward the axial direction. Inside the blade channel, shock/boundary-layer interaction leads to the formation of a λ shock and finally to boundary-layer separation. After further subsonic diffusion downstream of the shock, an outlet Mach number of 0.7 is obtained.

As further examples, Figs. 6-8 demonstrate some results of the rotor flow study within the blade channels at 100% compressor speed at 45% blade height. The mass flow through the stage again varies from the choke margin to compressor surge. In this case, the inflow Mach number is slightly supersonic. For the open throttle condition (Fig. 6), a

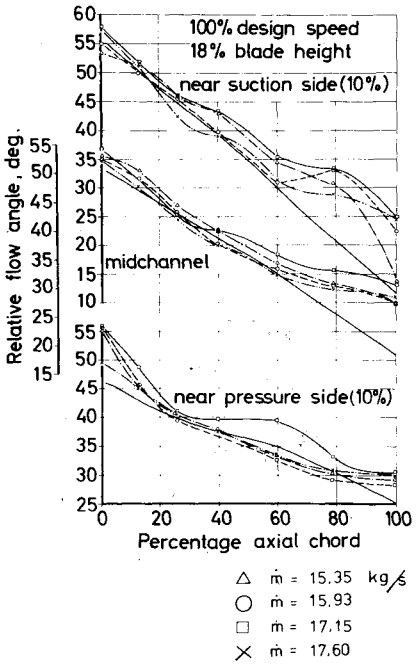

Fig. 12 Axial chordwise distribution of relative flow angle, deg, 100% speed, at 18% blade height.

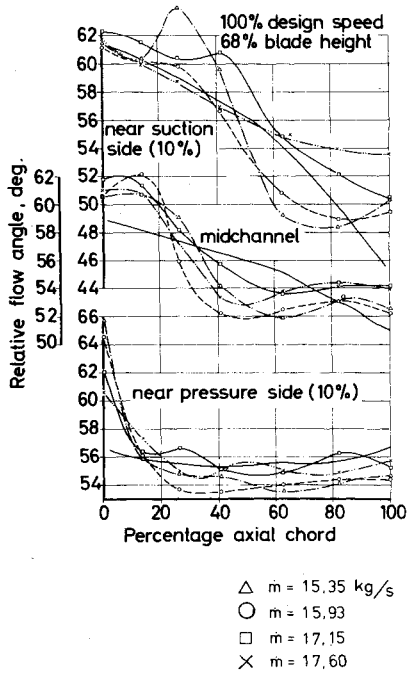

Fig. 13 Relative flow angle distribution as in Fig. 12, but at 68% blade height.

normal shock attached to the blade leading edge and a final shock within the blade passage can be observed. For the higher back-pressure conditions (Figs. 7 and 8), detached shock waves appear at the blade channel entrance.

Figures 9-11 show the relative Mach number distributions for the above mentioned mass flow rates at 89% blade height (near the blade tip). The inlet Mach number has increased up to 1.3. Noteworthy is the modification of the shock wave configurations with the corresponding mass flow rates. The diagrams presented here demonstrate typical flow phenomena within a transonic compressor rotor.

Another local flow study is illustrated in Figs. 12-14, which show the axial chordwise distribution of the relative flow angle through the rotor at three different blade heights. The

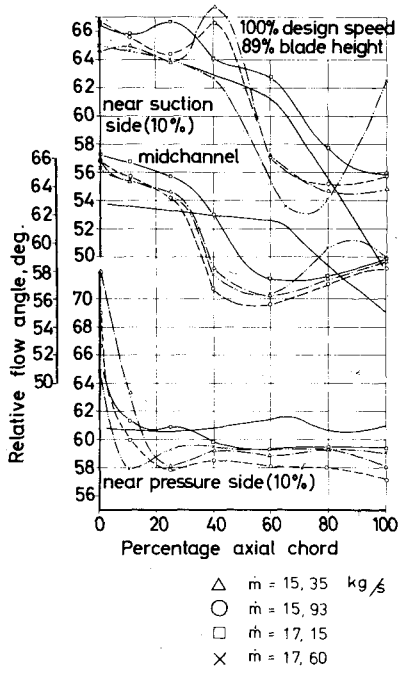

Fig. 14 Relative flow angle distribution as in Fig. 12, but at 89% blade height.

upper curves in each diagram represent the flow situation at 10% of blade pitch off the suction surface, the midcurves the flow at midchannel, and the lower curves the situation around 10% off the pressure side. The flow data are compared to the metal angle of the suction side, to the camberline angle, and to the pressure surface angle, all represented by solid lines (without symbols). The different mass flows were chosen to demonstrate the effect of compressor throttling.

Figure 12 shows the flow angle distribution at 18% blade height. The flow vectors follow the surface angles in the forward part of the blade passage quite accurately, except for the pressure surface near blade leading edge where high positive incidence angles occur. The variation of outlet flow angle is only about 2 deg for the four different throttle positions at this stream surface in the hub region.

In Fig. 13, the flow angles are shown at 68% blade height. The increase of the incidence angle, produced by throttling the compressor along the design speed line, is clearly obvious at the leading edge of the pressure surface (lower curves). Within the blade channel, the agreement between the pressure surface angles and the flow angles is quite good for the different mass flows, taking into account the 10% blade pitch distance. Near the suction side (upper curves) for the flow at 1.5% in mass flow off surge (Δ), the flow angle change at 25% axial chord results from the impinging of the normal shock on the suction surface boundary layer (see also Fig. 5). The shock/boundary-layer interaction brings about a thickening of the boundary layer, formation of a λ shock, and hence the alteration of the flow angle. At 7% in mass flow off surge (○), the change of flow turning direction is slightly smaller due to the lower Mach number before the shock. Also, for the peak efficiency point (□), an alteration of the flow angle takes place through the impinging normal shock at nearly 45% axial chord, whereas at open throttle condition (×), no severe flow turning occurs through the shock, as the loading of the boundary layer by the oblique shock is smaller. For all that, the flow seems to separate from the suction surface behind the shock for the latter two flow conditions, which is indicated by the discrepancy between flow and metal angles. Considering the flow turning along midchannel (middle curves), the distribution of the flow angle is quite different from the camberline angles for all four mass flow rates. The flow turning is completed nearly with the forward 60% axial

chord; beyond that point, a slightly negative turning occurs as in turbine operation. Once more, nearly the same outlet flow angle is reached for the best point as for conditions near compressor surge at the blade trailing edge on the pressure and suction sides and at midchannel.

Figure 14 presents the flow angle at 89% blade height with inflow Mach numbers about 1.3. On the pressure side, the main flow turning takes place along the forward portion of the blade, again due to the pressure surface incidence flow. Also, in midchannel, the whole flow turning is completed within the forward part of the channel. The distribution of flow turning is nearly the same for the flow situation at the open throttle condition and near the compressor surge, whereas the turning at the best point is delayed. Along the suction surface the flow angles clearly change through the impinging shock waves. At compressor choke margin, the flow at the blade outlet is deflected by an oblique shock, which is generated at the pressure side and extends downstream of the adjacent blade trailing edge into the outlet flow.

As described above in Figs. 12-14, the camberline angles and the flow directions at midchannel across the blade row differ considerably. This proved correct for the studied flow conditions at all blade heights. Therefore, measurements with the L2F technique have been performed in a cascade tunnel for the 45% blade section of the described compressor rotor. The results confirmed the difference between the camberline and the flow angles. Inviscid calculations yielded a similar result. This demonstrates that the camberline angle distribution is not representative for the flow turning through a blade channel. In contrast to the results of cascade investigations, where outlet flow angles change severely with back pressure and inflow conditions, the measured outlet flow angles downstream of this rotor differ only slightly at each blade height, at least for the flow conditions studied. The smallest differences are obtained near compressor surge for all investigated blade heights and not, as expected, for the peak efficiency point.

Figures 15-22 represent the flow studies downstream of the rotor in measuring plane 16 (see Fig. 1). Figures 15-17 show diagrams of span and pitchwise total temperature rise within the rotor illustrated by different finished areas. In addition, the blade trailing edge is plotted. With regard to Fig. 1, the axial distance between blade trailing edge and measuring plane 16 increases with radius, as does the relative outlet flow angle from hub to tip.

Figure 15 represents the enthalpy rise at open throttle. The region of high energy input clearly marks the blade wake. Due to the causes mentioned above, the wake is shifted against the rotating direction. The temperature rise is highest within the wake near the hub and casing. Considering the core flow, the energy input slightly decreases from hub to tip. At nearly 90% blade height, regions of very low temperature rise are found near the suction side wake where the temperatures are high.

Figure 16 demonstrates the situation at the compressor's best point, where obviously the energy input is nearly constant over the blade height and circumference. This result corroborates the design philosophy of this rotor. In the tip region, the enthalpy rise increases, as it has been designed to compensate for the wall losses. Again, the region of higher temperature rise represents the blade wakes.

Increased back pressure leads to the overall temperature rise at 1.5% off surge, as shown in Fig. 17. The wake region is enlarged at hub and tip, whereas at midchannel height, the difference between core flow and blade wakes is small. All high energy transfer is concentrated within the wake at hub and shroud.

Figures 18-22 show the fluctuating pressure and the circumferential total pressure loss distribution downstream of the transonic compressor rotor in plane 16 (see Fig. 1) at several blade heights. The oscillograms on the left in Fig. 18 represent the unsteady component of the absolute total pressure over nearly three blade passes at 30, 60, and 80% blade height and result from superimposing the pressure signal over 24 rotor revolutions. In the corresponding diagrams on the right, the unsteady component of the pressure (cleared of noise) is plotted as a function of time in the interval between successive blade passes at maximum efficiency. These pressure data combined with the velocity vectors measured with the laser anemometer can be used to calculate in detail the flow losses of the rotor. Superimposing the blade-to-blade distributions of the absolute total pressure, given by the addition of the steady and unsteady components (see Refs. 1 and 2) and the local absolute velocities, the static pressure distributions are calculated. Combining these and the relative velocities determined from the velocity triangles yields the pitchwise relative total pressures at several radii and, from this, the relative total pressure losses can be evaluated. As an

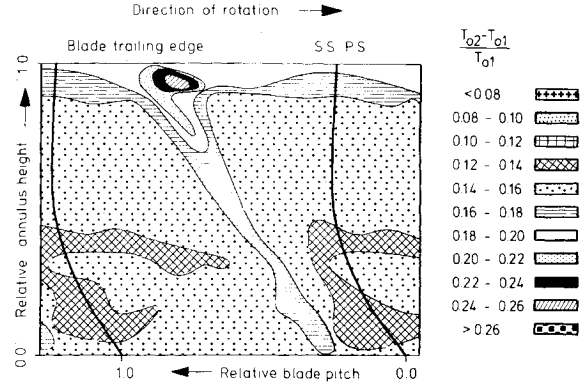

Fig. 16 Total temperature rise as in Fig. 15, but at maximum efficiency, $\dot{m} = 17.15$ kg/s.

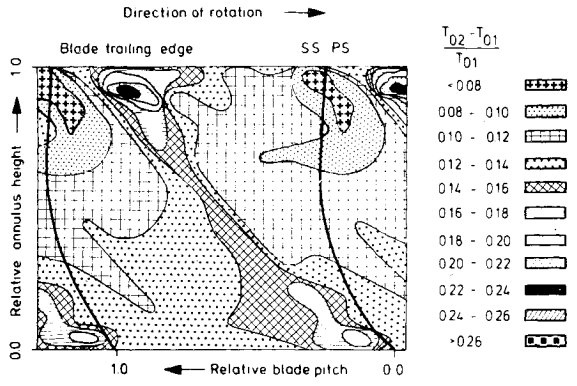

Fig. 15 Span and gapwise distribution of total temperature rise downstream of rotor in radial plane 16, 100% speed, compressor choke margin, $\dot{m} = 17.6$ kg/s.

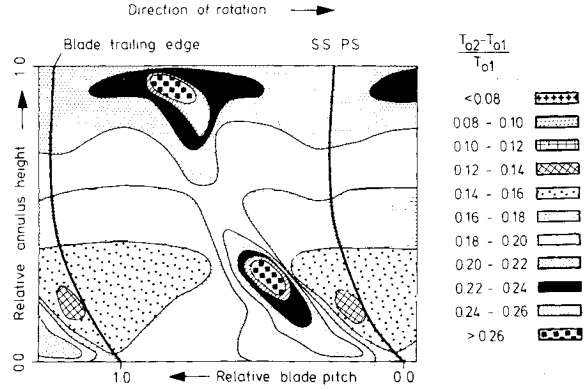

Fig. 17 Total temperature rise as in Fig. 15, but at 1.5% off surge, $\dot{m} = 15.35$ kg/s.

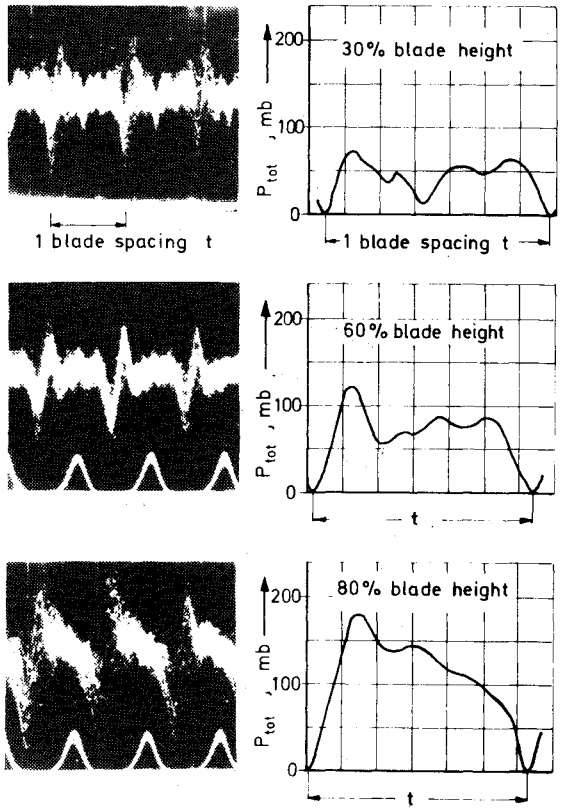

Fig. 18 Fluctuating total pressure (unsteady component) downstream of rotor, 100% speed.

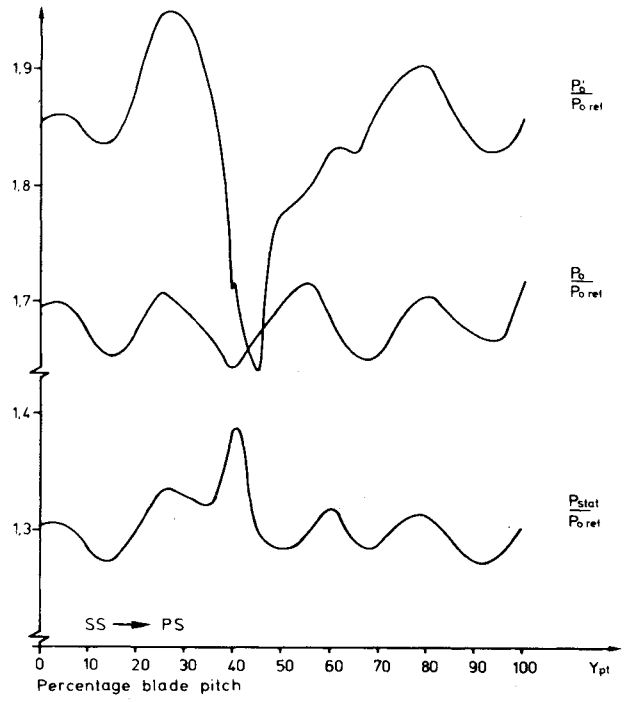

Fig. 19 Pitchwise distribution of normalized absolute and relative total pressure and static pressure downstream of rotor at 68% blade height, 100% speed, maximum efficiency, $\dot{m} = 17.15$ kg/s.

example, Fig. 19 illustrates the static and the total absolute and relative pressure distributions as a function of interblade distance at 68% blade height for the maximum efficiency point.

In Figs. 20-22, the above mentioned losses are plotted as circumferential distributions at three radii with respect to the position of the blade trailing edge. Figure 20 presents the loss

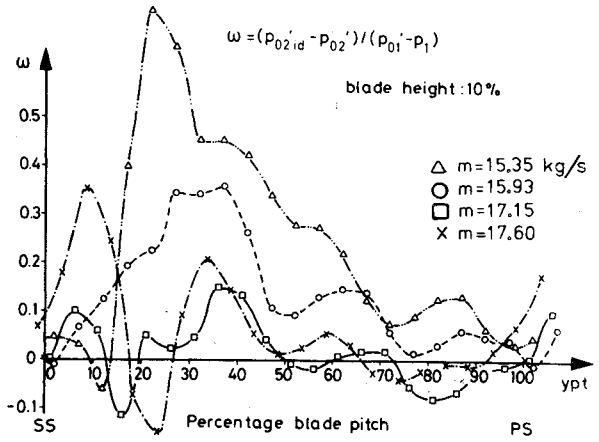

Fig. 20 Total pressure loss distribution across blade pitch from suction to pressure side with respect to blade trailing edge at 10% blade height.

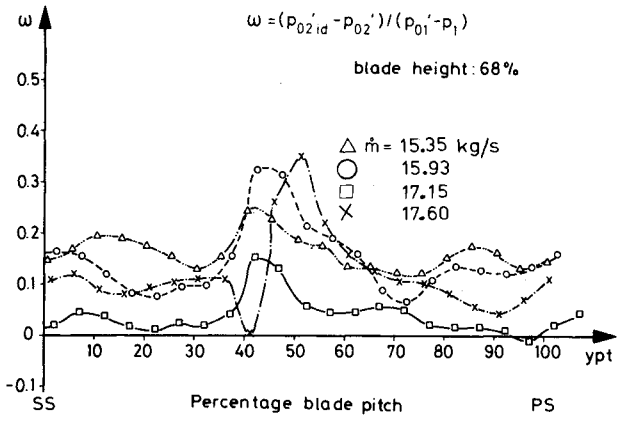

Fig. 21 Total pressure loss as in Fig. 20, but at 68% blade height.

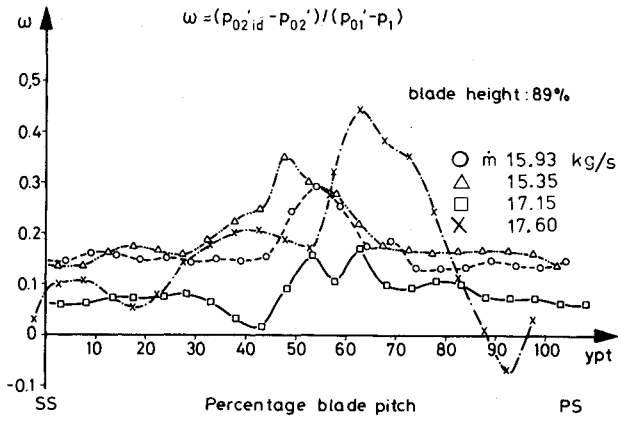

Fig. 22 Total pressure loss as in Fig. 20, but at 89% blade height.

curves at 10% blade height, i.e., near the hub. The negative loss values may seem surprising. It is not known whether these are based upon incorrect measurements or if they are possibly caused by corner vorticities. It should be emphasized, however, that it is rather difficult to measure the velocity gradient within the blade wake near the hub. Moreover, the question arises whether the steep gradient of the absolute total pressure from pressure to the suction side of the blades can be measured correctly with the probe setup used. In spite of these open questions, these results provide some interesting insights into the losses behind a rotating blade channel at different flow situations. The rotor losses for the flow condition at 1.5% in mass flow rate off surge (Δ) are highest, are

progressively less at 7% in mass flow off surge (o) and at the compressor's best point operation (□), and are somewhat larger than the minimum at compressor choke (×). Depending upon the four flow conditions, the position of the blade wake varies 25-35% of the blade pitch with respect to the relative position of the blade trailing edge. The loss distributions—as they are shown here—are quite typical for measurements in linear cascades.

In Fig. 21, the circumferential loss distribution is plotted at 68% blade height. At this flow condition, wall interferences are very small. Again, it is verified that the losses in total pressure are lowest for the compressor's best point (□). At the choke margin, they increase drastically, which is certainly due to the final normal shock impinging on the suction side trailing edge and causing a boundary-layer separation.

In Fig. 22, the losses are shown near the blade tip at 89% blade height. Again, the circumferential movement of the blade wake can be observed. The losses in the wake region at the choke condition are high, which may be caused by the interaction of the boundary layer with the final shock which extends downstream of the blade row.

Summary

The detailed investigations by means of the L2F velocimeter and the high-response pressure instrumentation give insight into the internal and downstream flow of a transonic axial compressor rotor along the design speed line at different flow conditions, ranging from open throttle to compressor surge.

The shock-wave system within the rotating blade rows was analyzed with respect to its position and intensity as a function of back pressure. The flow turning through the blade channels was studied and compared. The blade wakes were investigated from hub to tip, as well as the energy distribution downstream of the blades. In addition, information was obtained concerning shock/boundary-layer interaction and separation.

The radial and circumferential distributions of flow losses behind a rotating blade row were presented and described in detail. First steps were taken to investigate the prevailing uncertainty between cascade and rotor measurements. These studies will be developed in more detail to improve knowledge of loss models in axial compressors.

References

[1] Weyer, H. B., "The Determination of Time Weighted Average Pressures in Strongly Fluctuating Flows, Especially in Turbomachines," Technical Translation, European Space Research Organization, TT-161, 1974, p. 141.

[2] Weyer, H. B. and Hungenberg, H. G., "Analysis of Unsteady Flow in a Transonic Compressor by Means of High-Response Pressure Measuring Technique," AGARD-CP-177, 1976.

[3] Eckhardt, D., "Advanced Experimental Techniques for Centrifugal Compressor Development," Paper presented at ASME Fluid Dynamics Institute, *Radial Flow Turbomachinery Course,* Aug. 23-27, 1976, p. 135.

[4] Hantman, R. G., et al., "The Application of Holography to the Visualization of Shock Pattern in a Transonic Compressor," AIAA Paper 74-637, 1974.

[5] Epstein, A. H., "Quantitative Density Visualization in a Transonic Compressor Rotor," Ph.D. Thesis, M.I.T., Cambridge, Mass., Sept. 1975.

[6] Wisler, D. C. and Mossey, P. W., "Gas Velocity Measurements within a Compressor Rotor Passage Using the Laser Doppler Velocimeter," *Journal of Engineering for Power, Transactions of ASME*, Series A, Vol. 95, April 1973, p. 91.

[7] Walker, D. A., Williams, M. C., and House, R. D., "Intrablade Velocity Measurements in a Transonic Fan Utilizing a Laser Doppler Velocimeter," Paper presented at Minnesota Symposium on Laser Anemometry, Univ. of Minnesota, Minneapolis, Oct. 22-24, 1975.

[8] Wisler, D. C., "Shock Wave and Flow Velocity Measurements in a High Speed Fan Rotor Using the Laser Velocimeter," ASME Paper 76-GT-49.

[9] Schodl, R., "Laser Dual Beam Method for Flow Measurements in Turbomachines," ASME Paper 74-GT-157.

[10] Weyer, H. B. and Schodl, R., "Unsteady Flow Measurements in Turbomachines," *Modern Methods of Testing Rotating Components of Turbomachines*, AGARD-AG-207, 1975.

[11] Schodl, R., "On the Extension of the Range of Applicability of LDA by Means of the Laser-Dual Focus (L2F)-Technique," LDA-Symposium 1975, Technical University of Denmark, Copenhagen, Aug. 25-28, 1975.

[12] Strinning, P. E. and Dunker, R. J., "Aerodynamische und Schaufelauslegung einer Transsonischen Axialverdichterstufe," *Forschungsbericht Verbrennungskraftmaschinen,* Heft 178, 1975.

[13] Weyer, H. B., "Compressor Design and Experimental Results," and Weyer, H. B. and Dunker, R. J., "Comparison between the Calculated and the Experimental Results of the Compressor Test Cases," *Through-Flow Calculations in Axial Turbomachinery*, AGARD-CP-195, 1976.

[14] Dunker, R. J., Schodl, R., and Weyer, H. B., "Fortschritte in der Turbomaschinenforschung durch ein neues Optisches Meßverfahren für Strömungsvektoren," *Zeitschrift für Flugwissenschaft*, Heft 1, 1976, pp. 17-25.

[15] Dunker, R. J. and Strinning, P. E., "Flow Velocity Measurements Inside of a Transonic Axial Compressor Rotor by Means of an Optical Technique and Compared with Blade-to-Blade Calculations," *Proceedings of 3rd International Symposium on Air Breathing Engines*, Munich, DGLR-Fachbuch No. 6, March 7-12, 1976, pp. 217-232.

[16] Weyer, H. B. and Dunker, R. J., "Dual Beam Laser Anemometry Study of the Flow Field in a Transonic Compressor," *Secondary Flows in Turbomachines*, AGARD-CP-214, 1977.

[17] Dunker, R. J., et al., "Experimental Study of the Flow Field within a Transonic Axial Compressor Rotor by Laser Velocimetry and Comparison With Through-Flow Calculations," *Journal of Engineering for Power, Transactions of ASME*, Series A, Vol. 100, April 1978, p. 279.